Research Article

Optoelectronic, thermodynamic and vibrational properties of intermetallic MgAl$_2$Ge$_2$: a first-principles study

A. M. M. Tanveer Karim[1] · M. A. Helal[2] · M. A. Alam[3] · M. A. Ali[4] · I. Ara[5] · S. H. Naqib[5]

Abstract

Intermetallic compounds with CaAl$_2$Si$_2$-type structure have been studied extensively due to their exciting set of physical properties. Among various alumo-germanides, MgAl$_2$Ge$_2$ is the new representative of CaAl$_2$Si$_2$-type structures. Our previous study explores the structural aspects, mechanical behaviors and electronic features of intermetallic MgAl$_2$Ge$_2$. The present work discloses the results of optoelectronic, thermodynamic and vibrational properties of MgAl$_2$Ge$_2$ via density functional theory-based investigations. The band structure calculations suggest that MgAl$_2$Ge$_2$ possesses slight electronic anisotropy and the compound is metallic. The Fermi surface topology reveals that both electron- and hole-like sheets are present in MgAl$_2$Ge$_2$. The electron charge density map indicates toward the dominance of covalent bonding in MgAl$_2$Ge$_2$. The optical parameters are found to be independent of the state of the polarization of incident electric field. The large value of the reflectivity in the visible-to-ultraviolet region up to ~ 15 eV suggests that MgAl$_2$Ge$_2$ might be a good candidate as coating material to avoid solar heating. The thermodynamic properties have been calculated using the quasi-harmonic Debye approximation. We have found indications of lattice instability at the Brillouin zone boundary in the trigonal $P\bar{3}m1$phase from the phonon dispersion curves. However, the compound might be stable at elevated temperature and as a function of pressure. All the theoretical findings herein have been compared with the reported results (where available). Various implications of our results have been discussed in detail.

✉ A. M. M. Tanveer Karim, tanveerruphy@gmail.com; ✉ M. A. Helal, helalphy82@gmail.com | ^{1}Department of Physics, Rajshahi University of Engineering and Technology, Rajshahi 6204, Bangladesh. ^{2}Department of Physics, Begum Rokeya University, Rangpur 5400, Bangladesh. ^{3}Department of Physics, Mawlana Bhashani Science and Technology University, Santosh, Tangail 1902, Bangladesh. ^{4}Department of Physics, Chittagong University of Engineering and Technology (CUET), Chittagong 4349, Bangladesh. ^{5}Department of Physics, University of Rajshahi, Rajshahi 6205, Bangladesh.
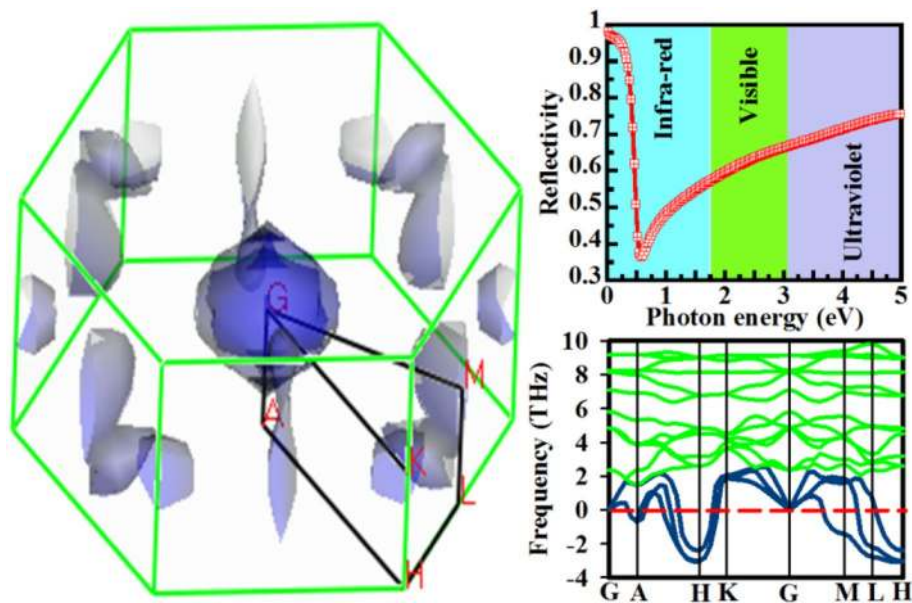
Graphic abstract

1 Introduction

Intermetallic compounds have been studied extensively over the last few decades due to their applications in different areas such as in optoelectronics, magnetism, spintronics and thermoelectrics. Intermetallic compounds with AM_2X_2-type formula, where A is the rare earth element, M refers to a metal and X is the element of the main group III, IV or V of the periodic table, belonging to the Zintl phase, crystallize mainly into the $ThCr_2Si_2$-type (tetragonal) structure and sometimes into the $CaAl_2Si_2$-type (trigonal) structure. Some of the Zintl phase compounds are promising thermoelectric materials because of their excellent structural stability at high temperatures and low thermal conductivity [1–6]. AM_2X_2-type intermetallics also exhibit attractive magnetic properties, and therefore, considerable research has been done by many groups on the magnetic aspects [7–10]. Due to the strong interaction between magnetism and charge transport properties, a slight change in external parameters such as temperature, pressure and magnetic field may cause a remarkable modification of their physical properties [11].

Among the AM_2X_2 compounds, $ThCr_2Si_2$-type and $CaCr_2Si_2$-type structured materials have been investigated thoroughly in the field of high-T_c superconductivity [12–17], the most common being the ternary pnictides

[18]. The most surprising behaviors of pnictides are that they tend to be antiferromagnetic [19], and superconductivity emerges with doping or under high pressures [18]. On the other hand, the Zintl phase with the $CaAl_2Si_2$-type structure has attracted a great deal of attention from the scientific community as thermoelectric materials. The transport properties of prototype $CaAl_2Si_2$ are controlled by both electrons and holes. Since their discovery, binary and ternary phases crystallizing in this structural pattern were challenging issues because of the stability limit [20]. Although it is very rare to develop $CaAl_2Si_2$-type structure, Pukas et al. [21] synthesized magnesium alumo-germanide ($MgAl_2Ge_2$) and confirmed its stable trigonal crystal structure by X-ray diffraction. The newly synthesized germanide is the third and last member in the Mg–Al–X (X = C, Si and Ge) system which belongs to the $CaAl_2Si_2$-type structure. In our previous work, we discussed the structural, electronic and elastic properties of this newly synthesized germanide in detail [22]. However, as far as we know, there is no report on the Fermi surface topography, charge density mapping, optical, thermodynamic and vibrational properties of $MgAl_2Ge_2$. Therefore, to bridge the existing research gap, we have undertaken the current project to investigate the above-mentioned unexplored properties in detail. Results obtained from the theoretical analysis reveal the suitability of $MgAl_2Ge_2$ as a potential material for future

optoelectronic-, thermodynamic- and vibrational-based intermetallic research.

## 2 Computational methodology

The first-principles calculations are carried out via the plane-wave pseudopotential method based on density functional theory which is implanted in CASTEP (CAmbridge Serial Total Energy Package) code [23]. The generalized gradient approximation by Perdew–Burke–Ernzerhof (GGA-PBE) [24] has been employed for calculating the exchange–correlation contribution to the electron–electron interaction. Vanderbilt-type ultrasoft pseudopotential was used. The plane-wave cutoff energy was 750 eV. For sampling the Brillouin zone, a Monkhorst–Pack grid of $16 \times 16 \times 8$ k-points was used. Geometry optimization was carried out using the convergence thresholds of 5×10^{-6} eV/atom for the total energy, 0.01 eVÅ^{-1} for the maximum force, 0.02 GPa for the maximum stress and 5×10^{-4} Å for the maximum atomic displacement. The vibrational properties were calculated using the DFPT linear response method [25]. The norm-conserving pseudo-approximation was used for obtaining temperature-dependent properties using DFPT. Different thermodynamic potential functions such as enthalpy, free energy and entropy of $MgAl_2Ge_2$ were calculated via quasi-harmonic Debye approximation.

The newly synthesized $MgAl_2Ge_2$ adopts a trigonal (space group $P\overline{3}m1$) crystal structure consisting of Mg atoms with a one-fold 1a Wyckoff position having fractional coordinates (0, 0, 0) which correspond to the Ca atoms in the structure of $CaAl_2Si_2$. On the other hand, Al and Ge atoms occupy two-fold sites in 2d Wyckoff position with fractional coordinates (1/3, 2/3, 0.6303) and (1/3, 2/3, 0.2404). The optimized crystal structure is shown in Fig. 1a. The lattice parameters of the optimized structure are $a = 4.130$ Å ($a^{expt} = 4.117$ Å) [21] and $c = 6.839$ Å ($c^{expt} = 6.787$ Å) [21]. Good correspondence between theoretical and experimental lattice parameters indicates the reliability of the present calculations.

3 Results and discussion

3.1 Energy band structure and Fermi surface

Fermi surface is a key characteristic to understand the charge transport properties of a compound. The Fermi surface topography can be derived from the electronic band structure. The electronic energy band structure of $MgAl_2Ge_2$ is presented in Fig. 1b. The energy band structure of $MgAl_2Ge_2$ has been displayed in the first Brillouin
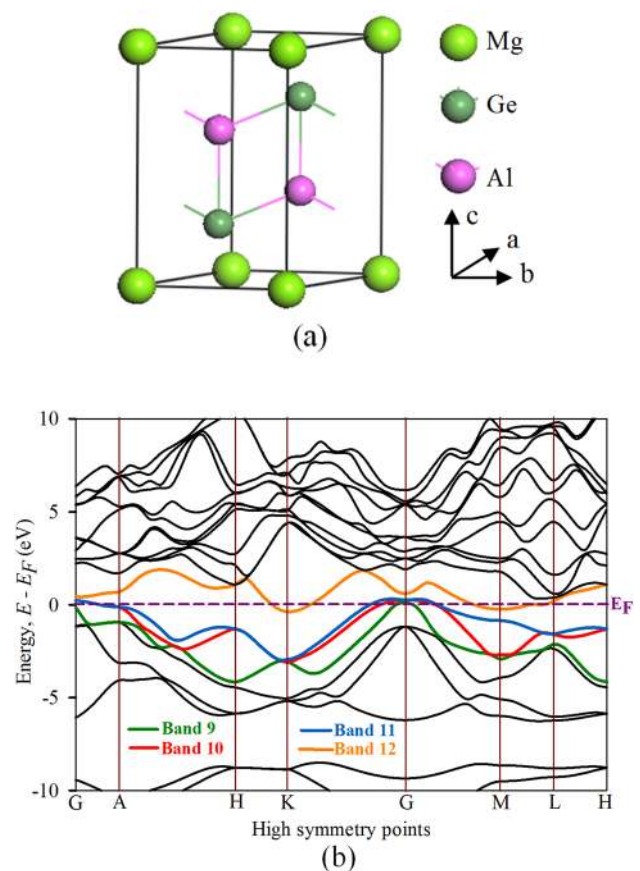
Fig. 1 **a** Crystal structure and **b** electronic band structure of $MgAl_2Ge_2$

zone along high symmetry directions. From Fig. 1b, it is seen that four valence bands (bands 9, 10, 11 and 12) cross the Fermi level (marked by the dark pink dashed line). Therefore, $MgAl_2Ge_2$ would display metallic behavior. Fermi surface of $MgAl_2Ge_2$ is shown in Fig. 2a–e. Both electron- and hole-like sheets are seen in these figures. Four Fermi sheets are produced for the four bands crossing the Fermi level. Band 9 produces an electron-like cylindrical Fermi sheet around the G point only. Band 10 produces another electron-like distorted spherical sheet along the G-A line only. Band 11 also produces a distorted spherical electron-like sheet along the G-M, G-K and G-A lines, and band 12 produces a hole-like sheet around the M-point and the K-point in the Brillouin zone. The deviation of Fermi sheets from free-electron sphere may be as a result of the effective Coulomb potential (attractive and repulsion) and non-isotropic crystalline state of $MgAl_2Ge_2$ [26]. However, the presence of both electron- and hole-like Fermi surfaces indicates the manifold band nature of intermetallic $MgAl_2Ge_2$. These multi-sheets are favorable for the enhancement of conductivity of $MgAl_2Ge_2$. The overall topography of the Fermi surface implies that
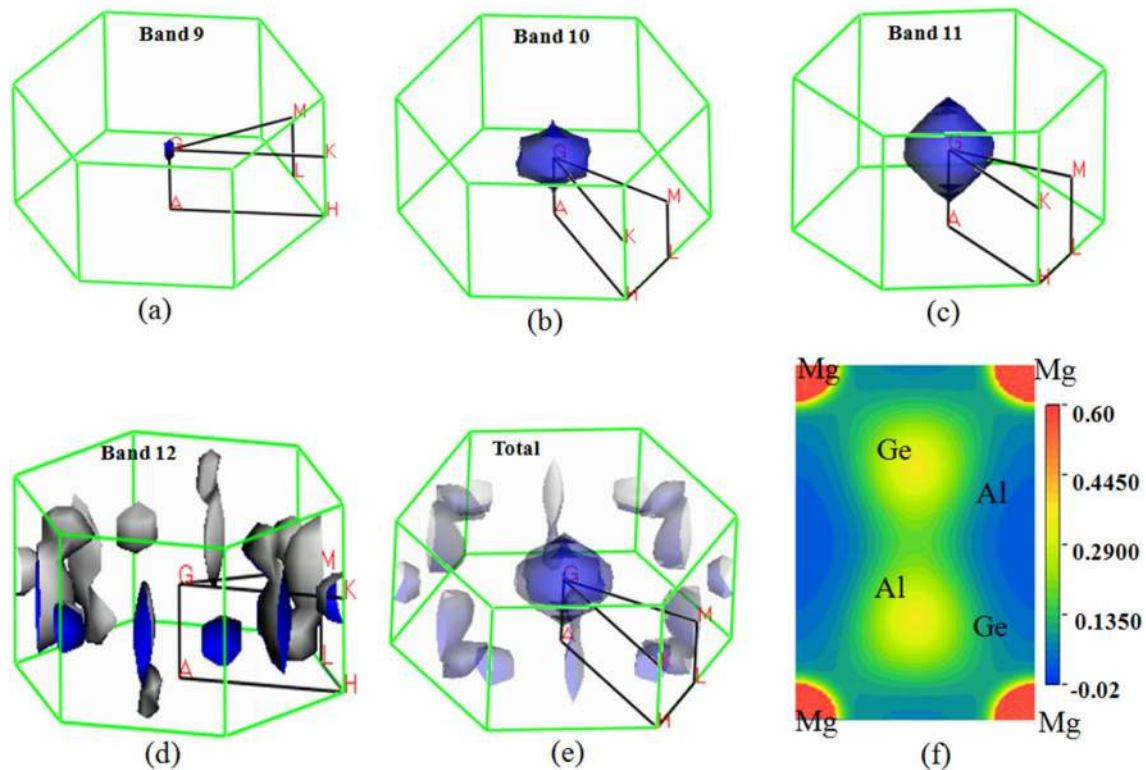
Fig. 2 **a–e** Fermi surface topology and **f** charge density distribution map in the (001) plane of MgAl$_2$Ge$_2$

charge conduction in the c-direction has electronic nature, while the conduction in the ab-plane is expected to show hole-like character. In addition, the pressure-dependent Fermi surface topological transition can cause the volume-dependent anomalies of phonon spectrum which may affect the thermodynamic properties of MgAl$_2$Ge$_2$.

3.2 Charge density distribution

The electron densities or accumulation of charges in different crystallographic planes are closely related to the nature of the atomic bonding in a compound. Therefore, charge density mapping can yield valuable information regarding the bonding character of MgAl$_2$Ge$_2$. The charge density mapping of MgAl$_2$Ge$_2$ based on charge density difference at different atomic sites is shown in Fig. 2f in the (001) crystallographic planes. The red and blue colors of the adjacent scale bar indicate the high and low density of electronic charge, respectively. The charge density map reveals the presence of Al–Ge, Mg–Ge and Al–Al covalent bonds in MgAl$_2$Ge$_2$. Among these covalent bonds, Al–Ge and Al–Al bonding seem to be stronger than the Mg–Ge bond. The lower covalent radii of Al and Ge may accumulate more electronic charges between themselves and

generate stronger covalent bonds than that between Mg and Ge atoms.

3.3 Optical properties

The study of the optical properties of a material is crucial to explore its potential for optoelectronic device applications. The optical response of a material to incident electromagnetic radiation is entirely determined by means of the various energy-dependent optical parameters such as absorption coefficient, reflectivity, refractive index, optical conductivity, loss function and dielectric constants. Figure 3a–f shows the calculated optical parameters of MgAl$_2$Ge$_2$ for photon energies up to 25 eV with electric field polarization vectors along [100] and [001] directions. We readily see from Fig. 3 that the optical parameters under study are fairly isotropic in nature; there are only slight differences in the positions and heights of the peaks with respect to the state of polarization of the incident electric field. A Gaussian smearing of 0.5 eV was used for all the calculations which integrates the k-points on the Fermi surface effectively. Since MgAl$_2$Ge$_2$ is metallic, both interband and intraband electronic transitions contribute to dielectric functions. Therefore, the Drude term with an
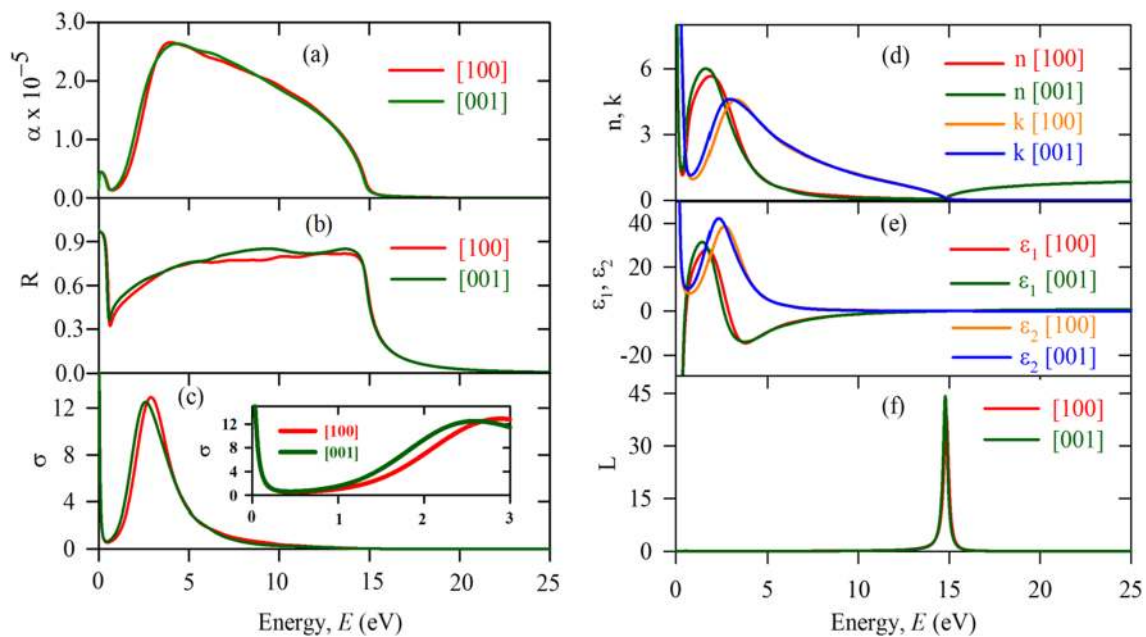
Fig. 3 **a** Absorption coefficient, **b** reflectivity, **c** optical conductivity, **d** refractive index, **e** dielectric constant and **f** loss function of $MgAl_2Ge_2$ electric field polarizations along [100] and [001] directions

unscreened plasma frequency 3 eV and damping 0.05 eV has been used for the low-energy part of the spectrum.

The energy-dependent absorption spectrum of $MgAl_2Ge_2$ is shown in Fig. 3a. The figure shows that $\alpha(\omega)$ increases sharply in the visible spectral range. The major peak in this spectrum, due to interband transition, is observed at around 4.0 eV i.e., in the near-ultraviolet (UV) region. The absorption of electromagnetic radiation begins from 0 eV reflecting the metallic character of $MgAl_2Ge_2$. It is interesting to note that, although the Ni-based germanide [27] absorbs the UV radiation quite effectively, the $MgAl_2Ge_2$ absorbs both the visible and UV radiation. Therefore, this material can be a promising absorber of electromagnetic radiation in both visible and UV regions.

The reflectivity, $R(\omega)$, profile of $MgAl_2Ge_2$ is shown in Fig. 3b. It is observed that $R(\omega)$ is above 90% and 44% in the infrared region and visible region, respectively. Li et al. [28] concluded that materials having the reflectivity ~ 44% or above in the visible spectral range are capable of minimizing solar heating. In the UV part of the electromagnetic spectrum, the reflectivity is non-selective over an extended energy range (5 eV–14 eV) and sustains a high value around 80%. A further increase in photon energy results in a sharp decrease in $R(\omega)$, and it becomes zero for energies greater than 15 eV. Therefore, $MgAl_2Ge_2$ can be used as a coating material for avoiding solar heat.

Figure 3c shows the photoconductivity $\sigma(\omega)$ spectrum of $MgAl_2Ge_2$. The photoconductivity is seen to start at zero

photon energy, indicating again that $MgAl_2Ge_2$ does not have a band gap in the electronic band structure. It is also observed that $\sigma(\omega)$ decreases at photon energy < 0.5 eV, grows up after and shows a sharp peak at ~ 2.50 eV. The decrease in σ for < 0.5 eV, its subsequent increase at higher energies and finally peaking at ~ 2.50 eV roughly follow the absorption coefficient spectrum within the same range of energy. This is an effect arising from the matrix element of photon-induced transitions of electrons between different energy states, controlled mainly by the product of electronic density of states at the energy levels involved.

The study of the refractive index is very important for materials due to its wide functional roles in the operations of different optical tools such as photonic crystals and waveguides [29]. The real, $n(\omega)$, and imaginary, $k(\omega)$, parts of the refractive index are displayed in Fig. 3d. The static value of the real part $n(0)$ is found to be 6.0. This particular parameter measures the phase velocity of light inside the compound. On the other hand, the imaginary part $k(\omega)$ measures the attenuation of light as it moves through the material. Metallic systems are characterized by high values of $k(\omega)$ for frequencies below the plasma edge.

Figure 3e illustrates the real, $\varepsilon_1(\omega)$, and imaginary parts, $\varepsilon_2(\omega)$, of the dielectric constant of $MgAl_2Ge_2$. As seen, both dielectric constants vanish at ~ 15 eV that corresponds to the photon energy at which the reflectivity (Fig. 3b) demonstrates a quick drop and energy loss function, $L(\omega)$ (describing the energy loss of a fast electron traversing the material), exhibits a very sharp peak as exposed in Fig. 3f.

Thus, the above facts fulfill the condition for plasma resonance at 15 eV. The negative value of the dielectric constant reflects the Drude-like behavior that is very common in metallic systems.

3.4 Thermodynamic properties

The correlations of thermodynamic parameters such as Debye temperature and specific heat with the elastic constants of materials allow us a profound understanding of the relationships between the mechanical and phonon structures. We have investigated the thermodynamic properties of $MgAl_2Ge_2$ by using the quasi-harmonic Debye model. The details regarding this model can be found elsewhere [30, 31]. In this section, we have calculated the Debye temperature, specific heat and volume thermal expansion coefficient at different temperatures ($T = 0$–1000 K) and pressures ($P = 0$–50 GPa). To do so, the Birch–Murnaghan equation of state [32] at zero temperature and pressure was used to fit the E–V data. In this work, the structure of $MgAl_2Ge_2$ has been optimized by varying the cutoff and k-points. At first, we have noted the energy and volume by taking a k-point mesh at different cutoff energy. After plotting, E–V data we have fixed the cutoff energy and noted the E and V for different k-point mesh. From these two plots, we have set the cutoff energy and k-point grid at minimum energy of the structure. The lattice of this particular structure is used for further calculations. The thermodynamic properties of a material can be obtained from the non-equilibrium Gibbs function $G^*(V;P,T)$ given by [30]

$$G^*(V;P,T) = E(V) + PV + A_{vib}[\Theta(V);T] \tag{1}$$

where $E(V)$ is the energy per unit cell, PV represents the pressure–volume product, $\theta(V)$ is the Debye temperature and the vibrational term A_{vib} can be expressed as

$$A_{vib}(\theta,T) = nkT\left[\frac{9\Theta}{8T} + 3\ln\left(1 - e^{-\frac{\Theta_D}{T}}\right) - D\left(\frac{\Theta_D}{T}\right)\right] \tag{2}$$

where n is the number of atoms per formula unit, k is the Boltzmann constant and $D\left(\frac{\Theta_D}{T}\right)$ is the standard Debye integral.

The Debye temperature (Θ_D) is an important lattice dynamical parameter. From the magnitude of Θ_D, one can infer to a number of physical parameters, namely specific heat, electrical and thermal conductivities, thermal expansion coefficient, etc. It is also related to the bonding strength among the atoms within the solids. The temperature- and pressure-dependent graphical presentations of Θ_D at different pressure and temperature are shown in Fig. 4a and b, respectively. It is seen from these figures that

the Θ_D decreases with increasing temperature, whereas Θ_D increases with increasing pressure which reflects that the thermal vibrational frequency of the atoms in this compound changes with temperature and pressure. One point is remarkable that at very low temperatures, Θ_D exhibits an overall saturation to a plateau. The existence of such a plateau is usually thought to be associated with zero-point vibration [33, 34]. We have calculated the Debye temperature using the Anderson method based on elastic constant in our previous study and found a value of 347 K [22]. This value is comparable with the value obtained from the quasi-harmonic Debye model.

The isothermal bulk modulus is a thermodynamic quantity which specifies the resistance to compression. The temperature dependence and pressure dependence of bulk modulus (B) of $MgAl_2Ge_2$ at different pressures and temperatures are shown in Fig. 5a and b, respectively. From Fig. 5a, it is observed that at zero pressure the bulk modulus of $MgAl_2Ge_2$ is found to decrease below 600 K; after that, it increases linearly. The increase in bulk
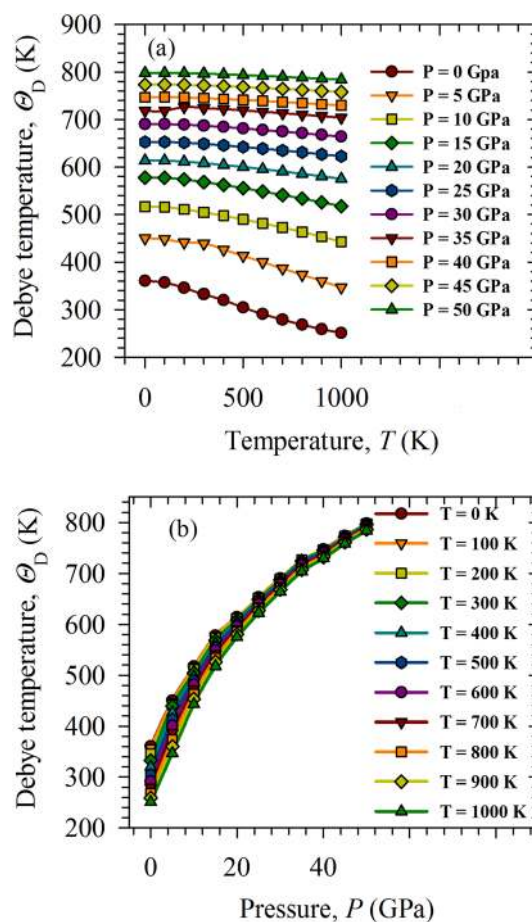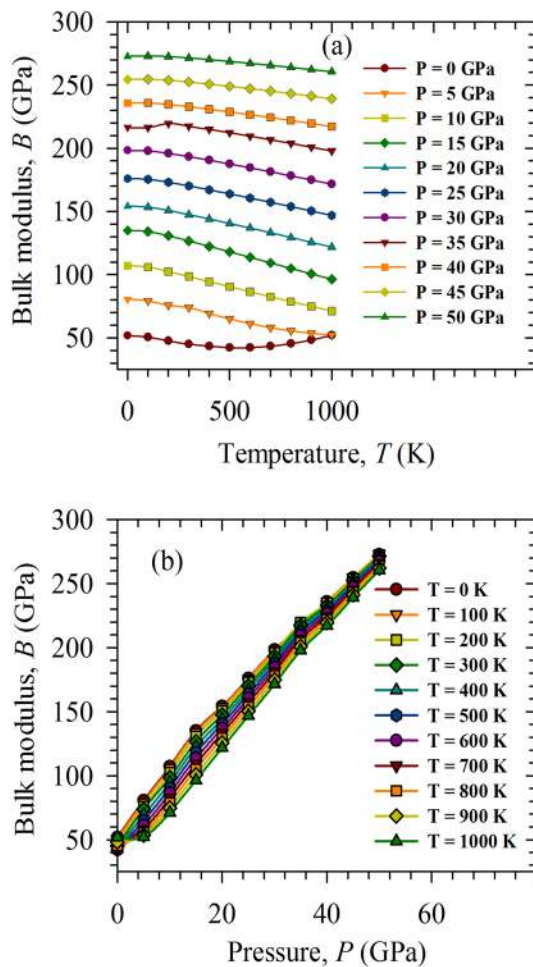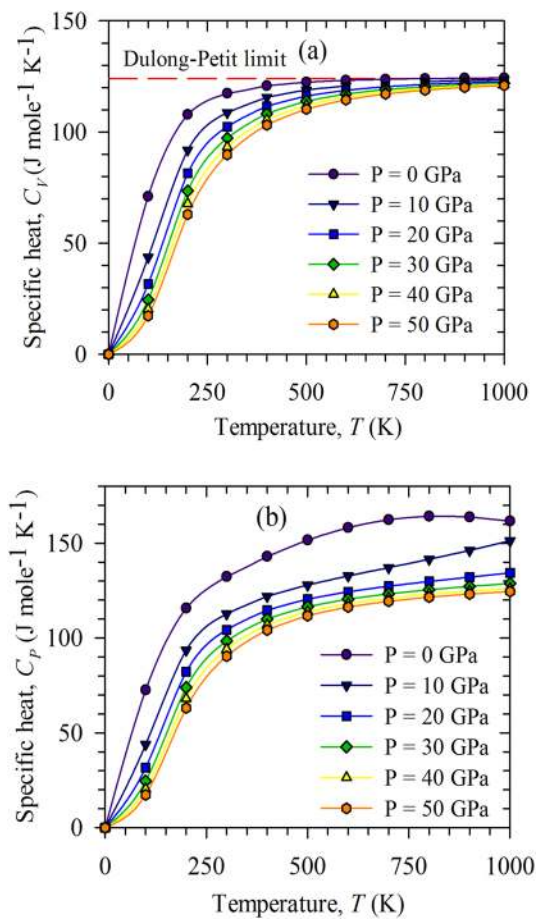

Fig. 4 Variation of Debye temperature of $MgAl_2Ge_2$ **a** with temperature at different pressures and **b** with pressure at different temperatures

Fig. 5 Variation of bulk modulus of MgAl$_2$Ge$_2$ **a** with temperature at different pressures and **b** with pressure at different temperatures

Fig. 6 Temperature dependence of **a** specific heat C_V and **b** specific heat C_P of MgAl$_2$Ge$_2$ at different pressures

modulus after 600 K is found to be altered in the presence of pressure. Moreover, bulk modulus diminishes slowly with temperature due to high pressure. The bulk modulus, in contrast, is found to increase significantly with increasing pressure at different fixed temperatures which is shown in Fig. 5b. The decrease in inter-atomic distance due to pressure increases in bulk modulus of MgAl$_2$Ge$_2$. This indicates that a decrease in pressure or an increase in temperature reduces the hardness of MgAl$_2$Ge$_2$.

The specific heat is an intensive property of material strongly correlated with temperature and pressure. The dependence of specific heat at constant volume (C_V) at different pressures is shown in Fig. 6a. It is observed that C_V increases as a function of temperature caused by phonon thermal softening. It is seen that pressure has a small influence on heat capacity. At sufficiently low temperatures, C_V follows the Debye-T^3 power law. However, at high temperature ($T > 500$ K), C_V approaches the classical Dulong–Petit limit (125 Jmole^{-1} K^{-1}) which is common to all solids at

high temperature. The same trend is observed for specific heat at constant pressure (C_P) and is shown in Fig. 6b.

Figure 7a and b shows the variation of volume thermal expansion coefficient (α_V) with temperature and pressure, respectively. It is seen from Fig. 7a that α_V increases rapidly with temperature up to 250 K but above 250 K the increment is gradual, suggesting that α_V is more sensitive to temperature at low temperature than at high temperature. However, the volume thermal expansion coefficient decreases strongly with pressure at a constant temperature as shown in Fig. 7b.
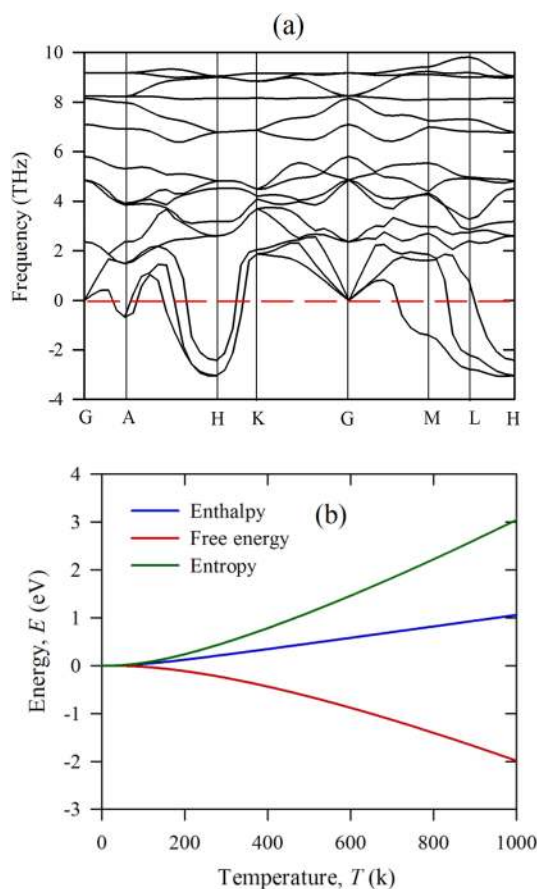
3.5 Vibrational properties

The phonon dispersion curves have been calculated along the direction of G-*A*-*H*-*K*-G-*M*-*L*-*H* in the first Brillouin zone, as shown in Fig. 8a. The phonon dispersion consists of three acoustic and twelve optical branches. Since the mass of Ge atom is much higher than Mg and Al, it can be said that Ge dominates the low-frequency phonon modes, while the contributions of Mg and Al are found at high
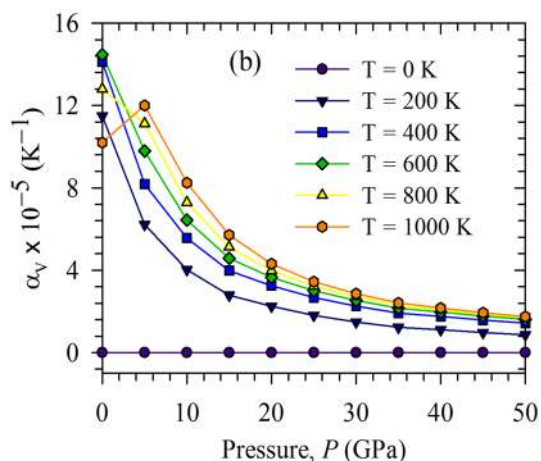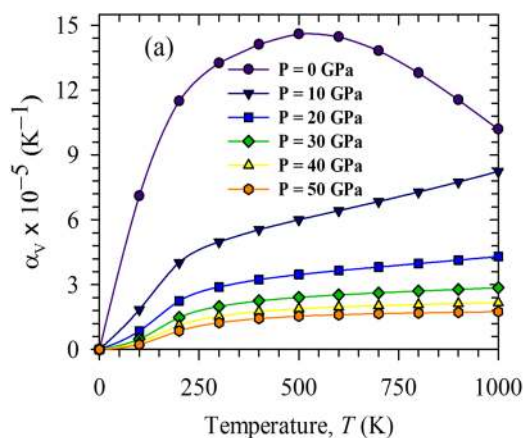
Fig. 7 Variation of volume thermal expansion coefficient of MgAl$_2$Ge$_2$ **a** with temperature at different pressures and **b** with pressure at different temperatures

Fig. 8 a Phonon dispersion curves and **b** temperature-dependent enthalpy, free energy and entropy of MgAl$_2$Ge$_2$

frequencies. The most striking feature of this spectrum concerns the lowest phonon branches which reach negative phonon frequencies at several points of the Brillouin zone. The negative values of the phonon frequencies correspond to dynamical failure of the crystal due to time-dependent perturbation. It should be noted that the computed phonon dispersion spectrum corresponds to absolute zero temperature. The situation at higher temperature can be different. Therefore, we predict that MgAl$_2$Ge$_2$ becomes dynamically unstable at low temperature, but it becomes stable at higher temperature. The imaginary modes of frequencies do not appear at high temperature since the compound has been already synthesized and no indication of lattice dynamical instability has been found [35]. The imaginary phonon modes at low-T indicate that MgAl$_2$Ge$_2$ might be susceptible to structural phase transition at low temperature. As far as we know, there is no available experimental or theoretical data on temperature-dependent structural parameters of MgAl$_2$Ge$_2$; therefore, conclusive remarks cannot be made. In the future, the

study of possible temperature or pressure dependence of structural phase transition could be an interesting topic.

Furthermore, thermodynamic behavior of MgAl$_2$Ge$_2$ can be described by some temperature-dependent potential functions such as enthalpy $H(T)$, Helmholtz free energy $F(T)$ and entropy $S(T)$. These thermodynamic parameters have been calculated at zero pressure using the quasi-harmonic approximation, where the Helmholtz free energy can be defined as $F(T) = H(T) - TS(T)$. The variation of enthalpy, free energy and entropy with temperature is shown in Fig. 8b. All these potential functions show almost zero values below 50 K. Above this temperature, both enthalpy and entropy increase significantly with increasing temperature, but Helmholtz free energy of MgAl$_2$Ge$_2$ varies in a reverse way.

4 Conclusions

$MgAl_2Ge_2$ is a new representative of $CaAl_2Si_2$-type structure among a variety of alumo-germanides. Previously, we disclosed the structural, mechanical and electronic properties of $MgAl_2Ge_2$. In this paper, we have studied Fermi surface topography, charge density distribution, optical, thermodynamic and lattice dynamical properties of intermetallic $MgAl_2Ge_2$ using the first-principles method based on density functional calculations. Electronic energy band structure confirms that $MgAl_2Ge_2$ is metallic. The Fermi surface shows both electron- and hole-like sheets indicating manifold band nature of $MgAl_2Ge_2$. Charge density mapping of $MgAl_2Ge_2$ indicates the presence of covalent bonds. Optical parameters do not exhibit significant optical anisotropy. The optical absorption and photoconductivity spectra started from zero photon energy as well as the large negative value of the dielectric constant indicates the metallic nature of $MgAl_2Ge_2$ which is also verified by energy band structure. The reflectivity spectra exhibit a sharp drop, and the energy loss function demonstrates a very sharp peak at 15 eV which is known as the plasma edge. From thermodynamic study, it is found that Debye temperature exhibits an overall saturation to a plateau at very low temperature which is usually thought to be associated with zero-point vibration. The hardness of $MgAl_2Ge_2$ is seen to vary both with temperature and with pressure. The specific heat at constant volume follows the Debye-T^3 power law at temperature below 500 K, after which approaches the classical Dulong–Petit limit of 125 $Jmole^{-1} K^{-1}$. The specific heat at constant pressure also follows the same trend. According to the phonon dispersion curves, indications regarding lattice instability were found around the Brillouin zone boundary at low temperature.

Since there are no experimental data on the studied properties of $MgAl_2Ge_2$ in this work, we anticipate that the obtained optoelectronic, thermal and vibrational properties of $MgAl_2Ge_2$ would serve as useful reference and stimulate future experimental and theoretical work to validate our results.

Compliance with ethical standards

Conflicts of interest There is no conflict to declare.

Availability of data The data that support the findings of this study will be available from the corresponding author upon reasonable request.

References

1. Zhang J, Song L, Iversen BB (2019) Insights into the design of thermoelectric Mg_3Sb_2 and its analogs by combining theory and experiment. Npj Compu Mats 5:76
2. Saparamadu U, Tan X, Sun J, Ren Z, Song S, Singh DJ, Shuai J, Jiang J, Ren Z (2020) Achieving high-performance p-type SmMg2Bi2 thermoelectric materials through band engineering and alloying effects. J Mater Chem A 8(31):15760–15766
3. Ohno S, Aydemir U, Amsler M, Pöhls JH, Chanakian S, Zevalkink A, White MA, Bux SK, Wolverton C, Snyder GJ (2017) Achieving zT > 1 in inexpensive zintl phase $Ca_9Zn_{4+x}Sb_9$ by phase boundary mapping. Adv Funct Mater 27(20):1606361
4. Guo M, Guo F, Zhu J, Yin L, Qin H, Zhang Q, Cai W, Sui J (2020) Enhanced thermoelectric properties of p-type $CaMg_2Bi_2$ via a synergistic effect originated from Zn and Alkali-metal co-doping. ACS Appl Mater Interf 12(5):6015–6021
5. Guo M, Zhu J, Guo F, Zhang Q, Cai W, Sui J (2020) Enhanced thermoelectric performance of P-type $CaMg_2Bi_{1.98}$ and optimized CaAl2Si2-type Zintl phase module with equal cross-section area. Mater Today Phys 15:100270
6. Ortiz BR, Gorai P, Stevanovic V, Toberer ES (2017) Potential for high thermoelectric performance in n-type Zintl compounds: a case study of Ba doped $KAlSb_4$. J Mater Chem A 5(8):4036–4046
7. Zheng C, Hoffmann R, Nesper R, Schnering HGV (1986) Site preferences and bond length differences in $CaAl_2Si_2$-type Zintl compounds. J Am Chem Soc 108(8):1876–1884
8. Cordier G, Schäfer HZ (1976) New intermetallic compounds in the anti-Ce_2O_2S-structure type. Naturforsch 31B:1459–1461
9. Shuai J, Mao J, Song S, Zhang Q, Chen G, Ren Z (2017) Recent progress and future challenges on thermoelectric Zintl materials. Mater Today Phys 1:74–95
10. Pakhira S, Tanatar MA, Johnston DC (2020) Magnetic, thermal, and electronic-transport properties of $EuMg_2Bi_2$ single crystals. Phys Rev B 101:214407
11. Banu IBS, Rajagopalan M, Yousuf M, Shenbagaraman P (1999) Electronic and bonding properties of ANi_2P_2 (A=Ca, Sr, Ba). J Alloys Comp 288(1–2):88
12. Sinaga GS, Utimula K, Nakano K, Hongo K,3, Maezono R. First principles calculations of superconducting critical temperature of $ThCr_2Si_2$-type structure. arXiv:1911.10716v1 . 2019
13. Iyo A, Ishida S, Fujihisa H, Gotoh Y, Hase I, Yoshida Y, Eisaki H, Kawashima K (2019) Superconductivity in uncollapsed tetragonal $LaFe_2As_2$. J Phys Chem Lett 10(5):1018–1023
14. Parvin F, Naqib SH (2019) Structural, elastic, electronic, thermodynamic, and optical properties of layered $BaPd_2As_2$ pnictide superconductor: a first principles investigation. J Alloys Comp 780:452–460

15. Rahman MA, Rahman MZ, Ali ML, Ali MS (2019) The physical properties of $ThCr_2Si_2$- type nickel-based superconductors $BaNi_2T_2$ (T = P, As): an ab-initio study. Chin J Phys 58:58–69

16. Zhang P, Hf Z (2017) Superconductivity in 122-Type pnictides without Iron. Condens Matter 2:28

17. Hadi MA, Ali MS, Naqib SH, Islam AKMA (2017) New ternary superconducting compound $LaRu_2As_2$: physical properties from density functional theory calculations. Chin Phys B 26(3):037103

18. Alireza PL, Ko YTC, Gillett J, Petrone CM, Cole JM, Lonzarich GG, Sebastian SE (2009) Superconductivity up to 29 K in $SrFe_2As_2$ and $BaFe_2As_2$ at high pressures. J. Phys Condens Mat 21(1):012208

19. Filsinger KA, Schnelle W, Adler P, Fecher GH, Reehuis M, Hoser A, Hoffmann JU, Werner P, Greenblatt M, Felser C (2017) Anti-ferromagnetic structure and electronic properties of $BaCr_2As_2$ and $BaCrFeAs_2$. Phys Rev B 95(18):184414

20. Zhang H, Zhao JT, Grin Y, Wang XJ, Tang MB, Man ZY, Chen HH, Yang XX (2008) A new type of thermoelectric material, $EuZn_2Sb_2$. J Chem Phys 129(16):164713

21. Pukas S, Pylypchak L, Matselko O, Demchenko P, Gladyshevskii R (2012) $MgAl_2Ge_2$ - a new representative of the structure type $CaAl_2Si_2$. Chem Met Alloys 5:59–65

22. Karim AMMT, Hadi MA, Alam MA, Parvin F, Naqib SH, Islam AKMA (2018) Newly synthesized $MgAl_2Ge_2$: a first-principles comparison with its silicide and carbide counterparts. J Phys Chem Sol 117:139–147

23. Segall MD, Lindan PJD, Probert MJ, Pickard CJ, Hasnip PJ, Clark SJ, Payne MC (2002) First-principles simulation: ideas, illustrations and the CASTEP code. J Phys Condens Mat 14:2717

24. Perdew JP, Burkey K, Ernzerof M (1997) Generalized gradient approximation made simple. Phys Rev Lett 78(7):1396

25. Refson K, Clark SJ, Tulip PR (2006) Variational density-functional perturbation theory for dielectrics and lattice dynamics. Phys Rev B 73(15):155114

26. Dugdale SB (2016) Life on the edge: a beginner's guide to the Fermi surface. Phys Scr 91:053009

27. Naefa MJ, Rahman MA (2019) Physical properties of $ThCr_2Si_2$-type Ni-based compounds $SrNi_2M_2$ (M= As and Ge): DFT based Ab-inito calculations. Phy C: Supercon Appl 560:19–25

28. Li S, Ahuja R, Barsoum MW, Jena P, Johansson B (2008) Optical properties of Ti_3SiC_2 and Ti_4AlN_3. Appl Phys Lett 92(22):221907

29. Russell P (2003) Photonic crystal fibers. Science 299(5605):358–362

30. Blanco MA, Francisco E, Luan V (2004) GIBBS: isothermal-isobaric thermodynamics of solids from energy curves using a quasi-harmonic Debye model. Comp Phys Commun 158(1):57–72

31. Hasan MZ, Hossain MM, Islam MS, Parvin F, Islam AKMA (2012) Elastic, thermodynamic, electronic and optical properties of U_2Ti. Compu Mater Sci 63:256–260

32. Birch F (1978) Finite strain isotherm and velocities for single-crystal and polycrystalline NaCl at high pressures and 300°K. Geophy J Res 83(B3):1257

33. Helal MA, Mori T, Kojima S (2015) Softening of infrared-active mode of perovskite $BaZrO_3$ proved by terahertz time-domain spectroscopy. Appl Phys Lett 106(18):182904

34. Muller KA, Burkard H (1979) $SrTiO_3$: an intrinsic quantum parae-lectric below 4 K. Phys Rev B 19(7):3593

35. Togo A, Tanaka I (2015) First principles phonon calculations in materials science. Scrip Mater 108:1–5